Title

Genetic Reduction of Matrix Metalloproteinase-9 Promotes Formation of Perineuronal Nets Around Parvalbumin-Expressing Interneurons and Normalizes Auditory Cortex Responses in Developing Fmr1 Knock-Out Mice.

Journal

Cerebral Cortex, 28(11)

ISSN

1047-3211

Authors

Wen, Teresa H
Afroz, Sonia
Reinhard, Sarah M
et al.

Publication Date

2018-11-01

DOI

10.1093/cercor/bhx258

Peer reviewed

Genetic Reduction of Matrix Metalloproteinase-9 Promotes Formation of Perineuronal Nets Around Parvalbumin-expressing Interneurons and Normalizes Auditory Cortex Responses in Developing *Fmr1* Knock-out Mice

Teresa H. Wen[a,b], Sonia Afroz[a], Sarah M. Reinhard[c], Arnold R. Palacios[a], Kendal Tapia[a], Devin K. Binder[a], Khaleel A. Razak[b,c,*] and Iryna M. Ethell[a,b, *]

[a]*Division of Biomedical Sciences, University of California Riverside School of Medicine, Riverside, California 92521, USA*

[b]*Neuroscience Graduate Program, University of California Riverside, Riverside, California 92521, USA*

[c]*Psychology Department and Psychology Graduate Program, University of California Riverside, Riverside, California 92521, USA*

**Co-corresponding Authors*

Correspondence:
Iryna M. Ethell, PhD
Division of Biomedical Sciences
University of California Riverside School of Medicine,
Riverside, California 92521, USA
Phone no: 951-827-2186
Facsimile no: 951-827-7121
iryna.ethell@medsch.ucr.edu

Running title: Restoring inhibition in developing auditory cortex of FXS mice

Conflict of Interest: The authors declare no competing financial interests.

ABSTRACT

Abnormal sensory responses associated with Fragile X Syndrome (FXS) and autism spectrum disorders include hypersensitivity and impaired habituation to repeated stimuli. Similar sensory deficits are also observed in adult *Fmr1* KO mice and are reversed by genetic deletion of Matrix Metalloproteinase 9 (MMP-9) through yet unknown mechanisms. Here we present new evidence

that impaired development of parvalbumin (PV)-expressing inhibitory interneurons may underlie hyper-responsiveness in auditory cortex of *Fmr1* KO mice via MMP-9-dependent regulation of perineuronal nets (PNNs). First, we found that PV cell development and PNN formation around GABAergic interneurons were impaired in developing auditory cortex of *Fmr1* KO mice. Second, MMP-9 levels were elevated in P12-P18 auditory cortex of *Fmr1* KO mice and genetic reduction of MMP-9 to WT levels restored the formation of PNNs around PV cells. Third, *in vivo* single unit recordings from auditory cortex neurons showed enhanced spontaneous and sound-driven responses in developing *Fmr1* KO mice, which were normalized following genetic reduction of MMP-9. These findings indicate that elevated MMP-9 levels contribute to the development of sensory hypersensitivity by influencing formation of PNNs around PV interneurons suggesting MMP9 as a new therapeutic target to reduce sensory deficits in FXS and potentially other autism spectrum disorders.

KEYWORDS

Autism, Cortical Plasticity, Extracellular Matrix, Fragile X Syndrome, Sensory hypersensitivity

Fragile X Syndrome (FXS) is a leading genetic cause of autism (Crawford et al., 2001). FXS is associated with a CGG trinucleotide repeat expansion in the Fragile X mental retardation (*Fmr1)* gene that leads to hypermethylation and loss of Fragile X mental retardation protein (FMRP; Yu et al., 1991). FMRP is an mRNA binding protein that regulates synaptic functions through protein translation (Darnell et al., 2011). Humans with FXS display cognitive and communication deficits, as well as delayed language development (Largo and Schinzel, 1985; Roberts et al., 2001), hyperarousal (Miller et al., 1999), abnormal social interactions (Hagerman

et al., 2009), sensory hypersensitivity and seizures (Wisniewski et al., 1991; Musumeci et al., 1999; Sabaratnam et al., 2001; Berry-Kravis, 2002). The *Fmr1* knock out (KO) mice display the core deficits of FXS, including sensory hypersensitivity and abnormal cortical processing (Chen and Toth, 2001; McNaughton et al., 2008; Gibson et al., 2008; Pietropaolo et al., 2011; Rotschafer and Razak, 2013; Lovelace et al., 2016).

Altered excitatory/inhibitory (E/I) balance may underlie abnormal cortical responses in humans with FXS and *Fmr1* KO mice, such as reduced habituation (Castrén et al., 2003; Lovelace et al., 2016; Ethridge et al., 2016, Wang, et al. 2017), hyper-responsiveness, broader receptive fields (Rotschafer and Razak, 2013, Arnett, et al. 2017; Zhang, et al. 2014) and increased network synchronization (Paluszkiewicz et al. 2011; Gonçalves et al., 2013; La Fata, et al. 2014). However, the cell- and network-specific changes underlying the E/I imbalance are only beginning to be understood (Gibson et al., 2008; reviewed in Contractor et al., 2015).

Normal development of fast-spiking parvalbumin (PV)-positive inhibitory interneurons is implicated in shaping 'critical period' plasticity, stabilization of synaptic networks and network synchronization (Hensch, 2005; Jeevakumar and Kroener, 2016). In the somatosensory cortex of *Fmr1* KO mice, there is decreased excitatory drive onto PV neurons and reduced PV expression (Selby et al., 2007; Gibson et al., 2008). Moreover, there is a down-regulation of $GABA_A$ receptor subunit α1 during postnatal cortical development in *Fmr1* KO mice (Adusei et al., 2010), a subunit normally enriched at PV cell/pyramidal cell synapses. Although these studies implicate PV cell dysfunctions in FXS-associated cortical hyperexcitability, the underlying mechanisms remain unclear.

Perineuronal nets (PNNs), which are extracellular matrix (ECM) components, are often associated with PV cells and regulate their development and functions. Loss of PNNs around PV

cells is associated with abnormal critical period plasticity and reduced excitability of PV cells (Pizzorusso et al., 2002; Balmer, 2016; Lensjø, et al. 2017). PNNs also protect PV cells against oxidative stress (Cabungcal et al., 2013). Matrix Metalloproteinase 9 (MMP-9) is a secreted endopeptidase, which regulates PNN formation and organization by cleaving ECM components (Ethell and Ethell, 2007). FMRP negatively regulates MMP-9 translation (Dziembowska et al, 2013) and MMP-9 levels are elevated in FXS (Bilousova et al., 2009; Sidhu et al., 2014; Gkogkas et al., 2014). MMP-9 deletion reverses several FXS phenotypes in *Fmr1* KO mice (Sidhu et al., 2014), including impaired auditory response habituation (Lovelace et al., 2016). However, it is unclear how enhanced MMP-9 activity may lead to auditory processing deficits in FXS.

Here, we hypothesized that increased MMP-9 levels affect auditory responses by influencing development of PNNs around PV cells in the auditory cortex of *Fmr1* KO mice. We found delayed development of PNNs and PV cells in layer 4 auditory cortex of *Fmr1* KO mice. PNN formation was selectively impaired around GABAergic PV interneurons but not excitatory neurons during the same period. *In vivo* single neuron recordings showed increased responses to tones in *Fmr1* KO mouse auditory cortex compared to WT mice at P21 suggesting impaired inhibition. While MMP-9 levels were reduced in the auditory cortex of WT mice after onset of hearing, MMP-9 levels remained elevated in developing auditory cortex of *Fmr1* KO mice at P12-18. Genetic reduction of MMP-9 levels restored auditory responses and the formation of PNNs around PV cells in the P21 *Fmr1* KO mice to WT levels. The concomitant changes in PV/PNN expression and electrophysiological responses following genetic reduction of MMP-9 in the *Fmr1* KO mice strongly suggest that elevated MMP-9 levels contribute to the development

of auditory processing deficits by influencing the development of PNNs and PV cells in the auditory cortex of *Fmr1* KO mice.

MATERIALS AND METHODS

Mice. FVB.Cg-*Mmp-9*^{tm1Tvu}/J and FVB.129P2-*Fmr1*^{tm1Cgr}/J (*Fmr1* KO) and FVB.129P2-Pde6b^{+}Tyr$^{c\text{-}ch}$/AntJ controls (WT) mice were obtained from Jackson laboratories and housed in an accredited vivarium on a 12h light/dark cycle. Food and water were provided *ad libitum.* The FVB.Cg-*Mmp-9*^{tm1Tvu}/J mice were backcrossed, in-house, with *Fmr1* KO mice to generate *Mmp9+/-Fmr1* KO mice, which had only one allele of the *Mmp9* gene and reduced expression of MMP-9. Genotypes were confirmed by PCR analysis of genomic DNA isolated from mouse tails. All procedures were approved by the Institutional Animal Care and Use Committee at the University of California, Riverside and carried out in accordance with NIH *Guide for the Care and Use of Laboratory Animals*.

Immunohistochemistry and image analysis. Age-matched male WT, *Fmr1* KO, and *Mmp9+/-Fmr1* KO mice at ages P14-15, P21-22, and P30-31 were euthanized with sodium pentobarbital or isoflurane and perfused transcardially with cold phosphate-buffered saline (PBS, 0.1 M) and 4% paraformaldehyde (PFA). Mmp9+/- *Fmr1* KO brain samples were collected and analyzed together with experimentally matched WT and *Fmr1* KO groups. Brains were removed and post-fixed for 2-4 h in 4% PFA. 100 µm sections were obtained using a vibratome (Leica S1000 or EMS 5000) with a speed of 2-2.5 and amplitude of 6-6.5. Auditory cortex was identified using hippocampal landmarks. This method has been previously validated using tonotopic mapping and dye injection (Martin del Campo et al., 2012) and comparison with the Paxinos mouse atlas and other publications on mouse auditory cortex (Anderson et al., 2009). Nevertheless, the

precise boundary between primary auditory cortex (A1) and anterior auditory field (AAF) of the mouse auditory cortex cannot be clearly established. Both these fields are part of the lemniscal auditory system and comprise the core auditory cortex. Therefore, we use the phrase 'auditory cortex' to indicate both A1 and AAF.

For each brain, an average of 5-6 slices containing auditory cortex were obtained. Sections were labeled using the following immunohistochemistry protocol. Briefly, brain slices were post-fixed for an additional 2 h in 4% PFA in 0.1M PBS and then washed in 0.1M PBS. Slices were then quenched with 50 mM ammonium chloride for 15 minutes and washed with PBS. Next, brain tissues were permeabilized with 0.1% Triton X-100 in PBS and nonspecific staining was blocked with a 5% Normal Goat Serum (NGS; Sigma, catalog# G9023-10mL) and 1% Bovine Serum Albumin (BSA; Fisher Scientific, catalog# 9048468) in 0.1 M PBS solution. Slices were then incubated for 24 h with primary antibodies and fluorescein-tagged *Wisteria floribunda agglutinin* (WFA) in 0.1 M PBS containing 1% NGS, 0.5% BSA, and 0.1% Tween-20 solution. WFA (4µg/ml; Vector Laboratories, cat# FL-1351, RRID:AB_2336875) is a lectin, which binds glycosaminoglycan side chains of chondroitin sulfate proteoglycans found in PNNs (Pizzorusso et al., 2002). Primary antibodies used include rabbit-anti PV (1:5000; SWANT, catalog# PV25, RRID:AB_10000344) or mouse anti-PV (1:1000; Sigma, catalog# P3088, RRID:AB_477329) to label PV interneurons and rabbit anti-GAD 65/67 (42.4µg/mL, Abcam, catalog#ab49832, RRID:AB_880149) to label all inhibitory interneurons. After incubation with primary antibodies and WFA, slices were washed in 0.1 M PBS containing 0.5% Tween-20 and incubated with secondary antibodies in 0.1M PBS for 1 h. Secondary antibodies were donkey-anti rabbit Alexa 594 (4µg/ml; Thermo Fisher Scientific, catalog# A-21207, RRID:AB_141637), donkey anti-rabbit Alexa 647 (4µg/ml; Thermo Fisher Scientific, catalog# A-31573,

RRID:AB_2536183) and donkey anti-mouse Alexa 594 (4µg/ml; Thermo Fisher Scientific, catalog# A-21203, RRID:AB_2535789). Slices were then washed with 0.1 M PBS containing 0.5% Tween-20, mounted with Vectashield containing DAPI (Vector Labs, catalog# H-1200) and Cytoseal (ThermoScientific, catalog# 8310-16). Slices were imaged by confocal microscopy (model LSM 510, Carl Zeiss MicroImaging or Leica SP5) using a series of 20 high-resolution optical sections (1024 x 1024-pixel format) that were captured for each slice using a 10x, 20x or a 63x water-immersion objective (1.2 numerical aperture), with 1x or 5x zoom at 1 um step intervals (z-stack). All images were acquired under identical conditions. Each z-stack was collapsed into a single image by projection (LSM Image Browser, Zeiss or Image J), converted to a TIFF file, encoded for blind analysis, and analyzed using Image J. Image J was also used to identify and count PNN positive cells, PV positive cells, GAD positive cells and colocalization. Cortical layers were identified (Anderson et al., 2009) and used for layer-specific counts. Cell counts were obtained in layers 1-5 of auditory cortex. The freehand selection tool and measure function was used to specify layers of the auditory cortex and the point tool was used to label PNNs, PV cells and GAD cells added to the ROI manager. Particle Analysis Cell Counter plugin in Image J was used to count colocalization. Two-way ANOVA was used to determine age and genotype differences. To characterize genotype differences, one-way ANOVA was used with Bonferroni *post-hoc* analysis for normally distributed data. Kruskal-Wallis one-way analysis of ranks was used with Dunnett's C for *post-hoc* analysis if data were not normally distributed. Statistical analyses were performed using GraphPad Prism 6.

Gelatin Zymography. P3, P7, P12, and P18 mice (n = 3-7 mice per group) were euthanized with isoflurane and the auditory cortex was dissected based on coordinates (Paxinos and Franklin, 2004) and previous electrophysiological and dye-placement studies (Martin del Campo et al.,

2012). The tissue samples were flash-frozen on dry ice and stored at -80° C. Gelatin gel zymography was performed as previously described with minor modifications (Sidhu et al., 2014). Briefly, auditory cortex tissue was re-suspended in 100 µL of 100 mM Tris-HCl (pH=7.6) buffer containing 150 mM NaCl, 5 mM $CaCl_2$, 0.05% Brij35, 0.02% Na_3N, 1% Triton X-100, 100 µM PMSF and PI cocktail (Sigma, catalog# P8340). Lysates were measured for total protein concentrations using the protocol for the BCA colorimetric protein assay (Pierce, 23235). The gelatinases, MMP-2 and MMP-9, were pulled down with gelatin agarose beads (Sigma, catalog# G5384) and separated on 10% Tris-Glycine gel with 0.1% gelatin as the substrate (Life Technologies). Following separation, gels were soaked in renaturing buffer (Life Technologies, catalog# LC2670) to remove all traces of SDS and allow the MMPs to refold thus regaining their enzymatic activity. Following renaturing, gels were incubated in developing buffer (Life Technologies, catalog# LC2671) for 96 h, allowing the gelatinases (MMP-2 and MMP-9) to degrade the gelatin in the gel. Gels were then stained with Coomassie Blue overnight to uniformly stain the gels after which de-staining revealed areas of MMP activity as unstained bands. Levels of MMP-2 and MMP-9 proteins were quantified by densitometry using Image J. For the analysis of developmental changes in MMP-2 and MMP-9 levels in P3, P7, P12 and P18 WT and *Fmr1* KO groups all values were normalized to P7 WT value on the same gel. For the analysis of MMP-2 and MMP-9 levels in MMP-9+/-*Fmr1* KO samples and experimentally matched WT and *Fmr1* KO groups, values for MMP-9+/-*Fmr1* KO and *Fmr1* KO samples were normalized against values for WT samples with similar protein concentration on the same gel. Statistical analysis was performed using ANOVA for comparison between the groups followed by Bonferroni *post hoc* pair-by-pair comparisons.

In vivo extracellular electrophysiology. Single unit recordings were obtained and analyzed using previously published methods to study adult mouse cortical responses (Rotschafer and Razak, 2013). Here age-matched (P13-16 and P19-23) male WT, *Fmr1* KO, *Mmp9+/-Fmr1* mice were anesthetized with a combination of 1g/kg urethane and 20mg/kg xylazine. Toe pinch reflex was monitored to ensure sufficient anesthesia levels and maintained with supplemental doses of urethane and xylazine. When mice were anesthetized, a midline incision was made to expose the skull. The temporalis muscle was reflected and a dental drill was used to create a cranial window to auditory cortex, which was identified using coordinates and vasculature.

Sounds were presented through free field speakers (Player BL Light; Avisoft, Gleinicke, Germany) maintained 7 inches and 45 degrees from the left ear. Single-unit extracellular electrophysiological recordings were obtained from the right auditory cortex (200-700um depth). While neural activity was recorded from all layers of auditory cortex, the majority of neurons were located in superficial layers (200-450um; P14: 62.5% of WT neurons, 73% of *Fmr1* KO neurons; P21: 55.68% of WT neurons, 69.23% of KO neurons, and 69.81% of *Mmp9+/-* neurons) and the distribution of neuron depths did not differ between WT and KO at P14, and WT, KO, and *Mmp9+/- Fmr1* KO mice at P21 (p=n.s.; Chi-square: Depth x Genotype). Tonotopy, short latency responses to pure tone stimuli, and vascular landmarks were used to find neurons in core auditory cortex. The frequency response of the sound delivery system, assessed with a 1 inch Bruel and Kjaer microphone and measuring amplifier, was flat within ± 4 dB between 5 and 40 kHz. The high frequency roll off was ~20 dB from 40-60 kHz. Acoustic stimulation and data acquisition were done with custom written software (Batlab; Dr. Dan Gans, Kent State University) and a Microstar digital processing board. Sound level was controlled using programmable attenuators (PA5; Tucker-Davis Technologies, Gainesville, FL).

Isolated neurons were probed with pure tones (5ms rise/fall time) in 1 or 5 kHz increments. Tones used were between 4 and 50 kHz as most neurons in the mouse core auditory cortex are tuned to <50 kHz (Rotschafer and Razak, 2013). Sound level was changed with 5 dB resolution to determine the characteristic frequency (CF), defined as the frequency at which a neuron responds at a minimum sound level. A tone at a specific frequency and level was counted as being excitatory if the neuron responded to at least three out five presentations. Response magnitude was compared in WT, *Fmr1* KO, and *Mmp9+/-Fmr1* neurons by generating a post-stimulus time histogram of responses to a 50 msec pure tone at the CF presented 15 dB above threshold (20 repetitions, 1 Hz repetition rate, 200 msec recording window from stimulus onset). Spontaneous activity was also recorded within 200 ms windows of silence that were interspersed between stimulus trials. The average spontaneous activity was calculated by dividing the total number of spikes recorded in silent windows divided by the number of repetitions of the silent window. At the end of the experiment, mice were euthanized with 125 mg/kg sodium pentobarbital. Statistical analysis was performed using Kruskal-Wallis one-way analysis of ranks and Dunnett's C was used for post-hoc analysis to characterize genotype differences as data were not normally distributed. To test for genotype and age effects in P14 and P21 response magnitudes, two-way ANOVA with Bonferroni post-hoc test was used.

RESULTS

PV cell development is impaired in the developing auditory cortex of *Fmr1* KO mice

The density of PV interneurons was analyzed in layers (L) 1-4 auditory cortex of WT and *Fmr1* KO mice at P14, P21 and P30 using immunohistochemistry (Fig 1A-I). A significant developmental increase in PV cell density was observed in both WT and *Fmr1* KO auditory cortex at P21 (Table 1; age effect, $p<0.01$). However, PV cell density was lower in the

developing *Fmr1* KO auditory cortex compared to WT (Table 1; genotype effect, $p<0.05$). Fluorescently tagged WFA was used to assess the density of PNN-containing cells in L1-4 auditory cortex (Fig 1A-I). Similar to PV cell density, a developmental increase in the density of PNN-enwrapped cells was observed in auditory cortex of *Fmr1* KO mice (age-effect, $p<0.001$, Table 1). PNN density in *Fmr1* KO auditory cortex did not reach WT levels until P30 (*Fmr1* KO P14 vs. P30, $p<0.001$, Table 1). Although there was a delay in PNN development in *Fmr1* KO auditory cortex, overall density of PNN-containing cells was not significantly different between genotypes. In summary, our results demonstrate reduced PV cell density in developing auditory cortex of *Fmr1* KO mice, and a delayed developmental increase in both PV and PNN-containing cells in *Fmr1* KO auditory cortex.

PNN formation is selectively impaired around PV interneurons in *Fmr1* KO auditory cortex at P21

Given a prominent accumulation of PNNs in L4 of sensory cortices and their abundance around PV cells in the adult cortex (Pizzorusso et al., 2002; Brewton et al., 2016), we next characterized layer-specific PV and PNN cell density in WT and *Fmr1* KO auditory cortex at P14, P21, and P30. PV cell density was lower in L4 *Fmr1* KO auditory cortex compared to WT at all ages (genotype effect, $p<0.05$; Fig. 1J). The difference was most prominent at P14, when we observed a significant reduction in PV cell density in both L2/3 and L4 Fmr1 KO auditory cortex compared to WT (L2/3, $p<0.0001$; L4, $p<0.05$; Fig. 1J). However, a developmental increase in PV cell density was only detected in L4 but not L2/3 of WT auditory cortex (WT, P14->P21, $p<0.01$; Fig. 1J). In addition, a developmental delay in PNN cell density was specifically observed in L4 *Fmr1* KO auditory cortex. PNN density was lower in L4 *Fmr1*

KO auditory cortex compared to WT mice at P14 ($p<0.0001$) and did not reach WT levels until P30 (Fig. 1K).

To determine if PNN formation was impaired around PV neurons, we analyzed the density of PNN/PV double-labeled cells and the percentage of PV cells containing PNN. We found that at P21 PNN formation was selectively impaired around PV cells in *Fmr1* KO auditory cortex compared to WT in both L2/3 ($p<0.01$) and L4 ($p<0.0001$; Fig. 1L). The percentage of PNN-containing PV cells was also reduced in L4 *Fmr1* KO auditory cortex compared to WT at P21 ($p<0.01$, Fig. 1M). Taken together, these data demonstrate developmental delays in PNN formation in L4 *Fmr1* KO auditory cortex, which can potentially affect PV expression and functions.

Reduced PNN formation around GABAergic interneurons in L4 *Fmr1* KO auditory cortex at P21

We next examined whether the reduction in PNN formation in L4 *Fmr1* KO auditory cortex was specific to GABAergic interneurons or if PNN formation was also impaired around non-GABAergic cells (Fig. 2A). A significant decrease in the density of GABAergic interneurons with PNNs was observed in *Fmr1* KO auditory cortex compared to WT at P21 (Fig. 2B; WT vs *Fmr1* KO, $p<0.01$). While PNN labeling was also detected around GAD65/67 negative cells (presumably excitatory neurons; arrowheads in Fig. 2C and D), there were no genotype differences in the density of PNN-containing cells lacking GAD65/67, indicating that impaired PNN formation was specific to GABAergic interneurons at P21. By P30 we no longer observed the differences in the density of PNN-containing GABAergic interneurons between WT and *Fmr1* KO auditory cortex (Fig. 2B). Taken together, these results show a delayed development of PNNs around GABAergic interneurons in L4 *Fmr1* KO auditory cortex

specifically at P21, which may lead to abnormal cortical development and underlie auditory processing deficits associated with FXS.

MMP-9 levels are higher in the developing auditory cortex of *Fmr1* KO mice

MMP-9 cleaves extracellular matrix and PNNs (Ethell and Ethell, 2007; Reinhard et al., 2015) and is elevated in FXS human brain and *Fmr1* KO mouse hippocampus (Dziembowska et al., 2013; Sidhu et al., 2014; Gkogkas et al., 2014), which may affect PNN development. Therefore, we first examined whether MMP-9 levels are elevated in developing auditory cortex of WT and *Fmr1* KO mice using a gelatin zymography assay. MMP-9 levels peaked in WT auditory cortex at P7 (Fig. 3A and B) just prior to hearing onset (Ehret, 1976; Kraus and Aulbach-Kraus, 1981). In WT auditory cortex, MMP-9 levels decreased at P12 and remained low at P18 (Fig. 3A and B; effect of age $p<0.009$), during the period of active PNN formation around PV cells and maturation of auditory cortex. While MMP-2 levels were not different between genotypes, MMP-9 levels were consistently elevated in *Fmr1* KO as compared to WT at all ages ($p<0.01$; Fig. 3A-C), suggesting that enhanced MMP-9 activity may impede PNN formation around PV interneurons in developing auditory cortex of *Fmr1* KO mice.

MMP-9 reduction promotes PNN formation around PV interneurons in layer 4 of *Fmr1* KO auditory cortex

To determine whether elevated MMP-9 levels contribute to abnormal PNN and PV cell development in *Fmr1* KO auditory cortex, we examined the effects of genetic reduction of MMP-9 on PV/PNN expression (Fig. 4A-C). At P12, MMP-9 levels were found to be significantly higher in *Fmr1* KO as compared to WT ($p<0.05$) and MMP-9+/-*Fmr1* KO ($p<0.01$, Fig. 3D, E), and were restored to WT levels in *Mmp9*+/-*Fmr1* KO auditory cortex. While genetic

reduction of MMP-9 levels did not affect the density of PV cells in *Mmp9*+/-*Fmr1* KO mice as compared to experimentally matched *Fmr1* KO mice (Fig. 4D), PNN density was significantly higher in layer 4 of *Mmp9*+/-*Fmr1* KO auditory cortex than in *Fmr1* KO at P21 ($p<0.0001$; Fig. 4E), even exceeding WT levels ($p<0.01$; Fig. 4E). The density of PV cells with PNN was also significantly higher in *Mmp9*+/-*Fmr1* KO auditory cortex compared to *Fmr1* KO at P21 ($p<0.01$; Fig. 4F). Moreover, the percentage of PV cells containing PNN was restored to WT levels in layer 4 of *Mmp9*+/-*Fmr1* KO auditory cortex at P21 and was significantly higher than in *Fmr1* KO ($p<0.001$; Fig. 4G). In contrast, we found no differences in the density of PV cells, PV cells with PNN, and the percentage of PV cells with PNNs in layer 5 of WT, *Fmr1* KO, and *Mmp9*+/-*Fmr1* KO auditory cortex (Supplementary Fig.1). These findings strongly suggest that abnormally high MMP-9 levels in the developing *Fmr1* KO mouse auditory cortex may primarily affect PNN formation around GABAergic PV interneurons in layer 4, which in turn may lead to reduced inhibition in the cortical network.

Response magnitudes are increased in developing auditory cortex of *Fmr1* KO mice

As the maturation of the synaptic and intrinsic properties of the mouse auditory cortex neurons occurs during the P12-P21 window (Oswald and Reyes, 2011; Kim, et al. 2013) and PNN disruption is known to reduce PV cell excitability and to affect excitatory/inhibitory balance in sensory cortex (Balmer, et al. 2016, Lensjø, et al. 2017), we hypothesized that *in vivo* responses of developing auditory cortical neurons to sounds will be also shifted towards more excitation in *Fmr1* KO mice. The magnitude of pure tone-evoked responses was compared between WT and *Fmr1* KO at P13-16 (P14 group) and P19-23 (P21 group), as deficits in PV expression were observed at P14, and reduced PV and PNN colocalization was prominent at P21 (Fig. 1, Fig. 4). Fig. 5A and D show example PSTHs in response to a 50 msec CF tone in WT

and *Fmr1* KO neurons at P14 and P21, respectively. At P14, response magnitude was not different between WT and KO mice (Fig. 5 B-E). However, at P21, *Fmr1* KO mice showed increased response magnitude across the entire 200 ms recording window compared to WT, as seen previously in adults (Rotschafer and Razak, 2013; *Fmr1* KO vs WT, $p<0.01$; Fig. 5E). When the recording window was split between the first 50ms onset response and the 51-200ms ongoing response, it was evident that differences were more influenced by changes in the ongoing response (Fig. 5B, C). *Fmr1* KO mice also exhibited age-related increase in spontaneous activity from P14 to P21 and more spontaneous activity in P21 *Fmr1* KO auditory cortex compared to WT (*Fmr1* KO mice P14 -> P21 $p<0.01$, *Fmr1* KO vs WT, $p<0.0001$; Fig 5F). These data indicate that responses become abnormally high between P14 and P21 *Fmr1* KO auditory cortex, a time window during which the PNNs mature around PV interneurons.

Genetic reduction of MMP-9 restores auditory cortex response magnitudes in *Fmr1* KO neurons to WT levels

Given that PNN formation around PV cells was restored to WT levels following genetic reduction of MMP-9 in Fmr1 KO mice at P21, we examined if single unit responses were also restored in auditory cortex of *Mmp9*+/-*Fmr1* KO mice. In order to test this, the magnitude of pure tone-evoked responses was compared between WT, *Fmr1* KO, and *Mmp9*+/-*Fmr1* KO neurons from P19-23 auditory cortex neurons. Fig. 6A shows example PSTHs in response to a 50 msec CF tone in WT (top), *Fmr1* KO (middle), and *Mmp9*+/-*Fmr1* KO (bottom) neurons. Responses were restored to WT levels with genetic reduction of MMP-9 levels in the *Mmp9*+/-*Fmr1* KO mice (Fig. 6B-D). The spontaneous activity was also significantly higher in the *Fmr1* KO mice compared to WT (*Fmr1* KO vs WT, $p<0.0001$; Fig. 6E) and was restored to WT levels with MMP-9 reduction (*Fmr1* KO vs. *Mmp9*+/-*Fmr1* KO, $p<0.0001$; Fig. 6E). Together, these

data show enhanced responses in the *Fmr1* KO mice compared to WT, and a restoration of normal responses by genetic reduction of MMP-9 in the *Mmp9*+/-*Fmr1* KO mice.

DISCUSSION

Auditory hypersensitivity is a common symptom in humans with FXS that may be related to abnormal sound evoked responses (Castrén et al., 2003; Van der Molen et al., 2012) and resting state hyperactive networks (Wang et al., 2017). Recent studies in humans with FXS (Ethridge et al., 2016, Wang et al., 2017) showed that abnormalities in sound evoked responses were correlated with heightened sensory sensitivity and autism-associated social impairment (Social Communication Questionnaire). Such symptoms are also prominent in autism spectrum disorders, in general (Sinclair et al. 2016). Sensory hypersensitivity may be driven by highly excitable cortical network activity that arises due to abnormal E/I balance (Rubenstein and Merzenich, 2003). Our previous studies showed hyperexcitable auditory cortical responses (Rotschafer and Razak, 2013) and impaired habituation to repeated sounds in adult *Fmr1* KO mice (Lovelace et al., 2016), suggesting impaired E/I balance. We show for the first time that *Fmr1* KO mice exhibit delayed development of PV interneurons and impaired PNN formation around PV interneurons in the developing auditory cortex. The deficits in PNN formation are most pronounced at P21 and are seen primarily in GABAergic PV neurons. Elevated MMP-9 levels most likely contribute to the deficits in developing *Fmr1* KO auditory cortex, as MMP-9 reduction in *Mmp9*+/-*Fmr1* KO mice restored PNN formation around PV interneurons and sound evoked and spontaneous activity to WT levels. These data implicate MMP-9 in the development of auditory cortex hyper-excitability in *Fmr1* KO mice via the regulation of PNN formation around PV interneurons and provide further support for targeting MMP-9 in treatment of FXS.

Fast-spiking PV cells are inhibitory interneurons implicated in shaping cortical E/I balance and network oscillatory activity relevant to sensory processing (Sohal et al., 2009; Cardin et al., 2009; Buzsáki and Wang, 2012). In our studies, impaired PNN formation around PV interneurons was observed in L2/3 and 4, but not L5 of the developing auditory cortex in *Fmr1* KO mice. L4 fast-spiking PV cells receive thalamic inputs (Winer et al., 2005) and provide feed-forward inhibition onto the thalamo-recipient pyramidal cells in L3 and 4 (Schiff and Reyes, 2012), which then project to L2/3, where signals are further refined (Douglas and Martin, 2004; Winer et al., 2005). PV-mediated inhibition in L2/3 is necessary for sharpening frequency receptive fields and helping to establish contrast of frequency representations (Li et al., 2014; Natan et al., 2015), both of which are impaired in *Fmr1* KO mice (Rotschafer and Razak, 2013; Kim et al., 2013). Involvement of PV interneurons in abnormal sensory processing in FXS is consistent with reduced excitatory drive onto PV interneurons and reduced PV expression in developing and adult somatosensory cortex of *Fmr1* KO mice (Selby et al., 2007; Gibson et al., 2008) and with abnormal resting gamma oscillations in humans with FXS (Wang et al., 2017), suggesting a broader role of PV neuron dysfunction in sensory abnormalities in FXS. These data are also consistent with altered PV cell function in other autism mouse models (Gogolla et al., 2009).

PNNs enwrap both inhibitory and excitatory neurons (Carulli et al., 2006), but we observed a selective loss of PNNs around PV-positive GABAergic interneurons at P21, with no differences observed in PNN expression around PV-negative neurons at P21. In addition to providing structural support (Brückner et al., 2000; Dansie and Ethell, 2011; Wlodarczyk et al., 2011), PNNs regulate survival (Morawski et al., 2004; Morawski et al., 2015; Cabungcal et al., 2013) and excitability of PV interneurons (Dityatev et al., 2007; Carulli et al., 2010; Balmer,

2016), and stabilization of sensory circuits (Pizzorusso et al., 2002; McRae et al., 2007). PNNs also regulate PV cell maturation via internalization of homeoprotein Otx2, which is needed for transcription, normal PV development and critical period plasticity in developing visual cortex (Sugiyama et al., 2008). Chondroitinase ABC, an enzyme that cleaves PNN proteoglycans, reduces $GABA_A$ inhibitory postsynaptic currents (Liu et al., 2013) and reduces excitability of PV fast spiking cortical interneurons (Balmer, 2016). Thus the loss of PNN around PV cells may lead to impaired maturation, survival and/or reduced excitability of PV neurons and overall loss of inhibition in the network leading to FXS-related sensory hypersensitivity.

While delayed PNN formation may contribute to enhanced excitability in P21 *Fmr1* KO mice, this does not explain impaired PV cell development that occurs during early PNN formation at P14. This early reduction in the number of PV cells may occur due to abnormal interneuron differentiation and migration during embryonic development (Castrén et al., 2005; reviewed in Castrén 2016). FMRP is especially important for normal fate determination of radial glia, known progenitors of both excitatory and inhibitory neurons in the cortex (Tervonen et al., 2009; Saffary and Xie, 2011). FMRP may regulate PV cell fate through translational control of transcription factors necessary for GABAergic neuron differentiation (reviewed in Sultan, et al. 2013). Although we see reduced PV density in *Fmr1* KO auditory cortex at P14, no differences in spontaneous and evoked responses were observed between WT and KO at P14. Auditory hypersensitivity developed between P14 and P21, which coincides with a critical window for E/I balance maturation and PNN formation in the auditory cortex. Therefore, hypersensitive neural circuits are not present around the time of hearing onset in the *Fmr1* KO mice, but develop between P14 and P21 suggesting a window for potential treatment of sensory hypersensitivity. Our results also suggest that reduced PV expression alone at P14 do not cause increased response

magnitudes in the *Fmr1* KO mice, but the abnormal maturation of PNN, likely driven by high MMP-9 levels, drive single-unit hyperexcitability at P21.

The abnormally high MMP-9 levels, altered PV/PNN development and increased responses that we observed in *Fmr1* KO auditory cortex occur during a critical window of auditory cortex development in mice. Intrinsic properties of PV inhibitory interneurons undergo major changes during P10-P29 period of early postnatal development. Younger P10-19 PV cells exhibit broader action potentials, longer after-hyperpolarizations, and higher adaptation ratios, resulting in overall reduced firing rates as compared to older P19-29 PV cells. Investigation of synapses between PV and pyramidal neurons also demonstrate age-related reduction of IPSP rise, peak, and decay time between P10-19 and P19-29 (Oswald and Reyes, 2011). *Fmr1* KO neurons exhibit increased response magnitudes and spontaneous activity and PV/PNN deficits during this developmental window that coincides with the maturation of cortical inhibition. Taken together, these data indicate that increased single neuron hyperexcitability in *Fmr1* KO auditory cortex may arise from delayed maturation of PV neurons, which can occur with disruption of PNNs. The lower PV/PNN density and reduced network inhibition during early development is also consistent with altered critical period plasticity observed in the auditory cortex of *Fmr1* KO auditory cortex (Kim, et al., 2013, Hensch 2005).

Another major finding presented here is that developmental delay in PNN formation in *Fmr1* KO auditory cortex may be attributed to elevated MMP-9 levels, as genetic reduction in MMP-9 levels was able to reverse abnormal PNN formation around PV cells and to restore auditory response magnitude at P21. In addition, we found a significant reduction in PV expression and PV/PNN colocalization in MMP-9 -/- mice (not shown), which is consistent with MMP-9 role in neurodevelopment (reviewed in Reinhard et al., 2015), suggesting that too much

or too little MMP-9 would affect PV cell development. Therefore, instead of deleting or reducing MMP-9 below the normal levels, in these studies we examined the effects of restoring MMP-9 to WT levels in *Fmr1* KO mice. This approach is also closer to our goal of developing future therapeutic approaches to restoring MMP-9 to WT levels in FXS. Excessive MMP proteolytic activity may affect formation of ECM and PNNs by cleaving its link proteins, such as laminin, fibronectin and aggrecan (D'ortho et al., 1997). The role of ECM in cortical plasticity has been previously reported (Pizzorusso et al., 2002; Nagy et al., 2006; McRae et al., 2007; Rivera et al., 2010), but the effects of elevated MMP-9 on cell and network function in FXS are still unclear. MMP-9 levels are elevated in FXS human brains and the hippocampus of *Fmr1* KO mice (Dziembowksa et al., 2013, Sidhu et al., 2014; Gkogkas et al., 2014). Here we report that MMP-9 levels are also elevated during a developmental sensitive window in *Fmr1* KO auditory cortex, whereas genetic reduction of MMP-9 in *Fmr1* KO mice rescues observed PNN deficits and restores response magnitudes and spontaneous activity to WT levels. Genetic deletion of MMP-9 rescues several other FXS phenotypes, including improper dendritic spine maturation, enhanced mGluR5-dependent-LTD, abnormal social behavior and macroorchidism (Sidhu et al., 2014). On the other hand, MMP-9 overexpression mimics FXS phenotypes, resulting in immature spine development, social behavior deficits and macroorchidism (Gkogkas et al., 2014). Elevated MMP-9 levels in *Fmr1* KO auditory cortex are most likely responsible for the developmental delay in PNN formation around PV cells during auditory cortex development and is at least partially responsible for auditory processing deficits. Our studies provide a novel mechanistic insight into sensory hyper-responsiveness in FXS taking into account early developmental circuit changes and emphasize the importance of MMP-9 and PNNs in normal auditory cortex development.

FUNDING SOURCES

This work was supported by the National Institutes of Health (NIH) (1U54 HD082008-01 to I.M.E., D.K.B., and K.A.R.); US Army Medical Research (W81XWH-15-1-0436 to I.M.E., D.K.B., and K.A.R.); and the NSF graduate research fellowship program (to S.R.).

ACKNOWLEDGEMENTS

We thank members of the Ethell, Binder and Razak laboratories for helpful discussions. We also thank David Carter for advice on confocal microscopy.

REFERENCES

Adusei DC, Pacey LK, Chen D, Hampson DR. 2010. Early developmental alterations in GABAergic protein expression in fragile X knockout mice. Neuropharmacology. 59: 167-171.

Anderson LA, Christianson GB, Linden JF. 2009. Mouse auditory cortex differs from visual and somatosensory cortices in the laminar distribution of cytochrome oxidase and acetylcholinesterase. Brain Res. 1252: 130-142.

Arnett MT, DH Herman, AW McGee. 2014. Deficits in tactile learning in a mouse model of fragile X syndrome. PloS one. 9: e109116.

Balmer TS. 2016. Perineuronal Nets Enhance the Excitability of Fast-Spiking Neurons. eNeuro. 3: 1-13.

Berry-Kravis E. 2002. Epilepsy in fragile X syndrome. Dev Med Child Neurol. 44: 724-728.

Bilousova TV, Dansie L, Ngo M, Aye J, Charles JR, Ethell DW, Ethell IM. 2009. Minocycline promotes dendritic spine maturation and improves behavioral performance in the fragile X mouse model. J Med Genet. 46: 94-102.

Brewton DH, Kokash J, Jimenez O, Pena ER, Razak KA. 2016. Age-related deterioration of perineuronal nets in the primary auditory cortex of mice. Front Aging Neurosci. 8: 270.

Brückner G, Grosche J, Schmidt S, Härtig W, Margolis RU, Delpech B, Seidenbecher CI, Czaniera R, Schachner M. 2000. Postnatal development of perineuronal nets in wild‐type mice and in a mutant deficient in tenascin‐R. J Comp Neurol. 428: 616-29.

Buzsáki G, Wang XJ. 2012. Mechanisms of gamma oscillations. Annu Rev Neurosci 35: 203.

Cabungcal JH, Steullet P, Morishita H, Kraftsik R, Cuenod M, Hensch TK, Do KQ. 2013. Perineuronal nets protect fast-spiking interneurons against oxidative stress. Proc Natl Acad Sci. 110: 9130-9135.

Cardin JA, Carlén M, Meletis K, Knoblich U, Zhang F, Deisseroth K, Tsai LH, Moore, CI. 2009. Driving fast-spiking cells induces gamma rhythm and controls sensory responses. Nature. 459: 663–667.

Carulli D, Rhodes KE, Brown DJ, Bonnert TP, Pollack SJ, Oliver K, Strata P, Fawcett JW. 2006. Composition of perineuronal nets in the adult rat cerebellum and the cellular origin of their components. J Comp Neurol. 494: 559-77.

Carulli D, Pizzorusso T, Kwok JCF, Putignano E, Poli A, Forostyak S, Andrews MR, Deepa SS, Glant TT, Fawcett JW. 2010. Animals lacking link protein have attenuated perineuronal nets and persistent plasticity. Brain. 133: 2331–2347.

Castrén M, Pääkkönen A, Tarkka IM, Ryynänen M, Partanen J. 2003. Augmentation of auditory N1 in children with fragile X syndrome. Brain Topogr. 15: 165-171.

Castrén M, Tervonen T, Kärkkäinen V, Heinonen S, Castrén E, Larsson K, Bakker CE, Oostra BA, Akerman K. 2005. Altered differentiation of neural stem cells in fragile X syndrome. Proc Natl Acad Sci USA. 102: 17834-17839.

Castrén ML. 2016. Cortical neurogenesis in fragile X syndrome. Front Biosci (Scholar edition). 8: 160.

Chen L, Toth M. 2001. Fragile X mice develop sensory hyperreactivity to auditory stimuli. Neuroscience. 103: 1043-1050.

Contractor A, Klyachko VA, Portera-Cailliau C. 2015. Altered Neuronal and Circuit Excitability in Fragile X Syndrome. Neuron. 87: 699-715.

Crawford DC, Acuña JM, Sherman SL. 2001. FMR1 and the fragile X syndrome: human genome epidemiology review. Genet Med. 3: 359–371.

D'ortho M-P, Will H, Atkinson S, Butler G, Messent A, Gavrilovic J, Smith B, Timpl R, Zardi L, Murphy G. 1997. Membrane-type matrix metalloproteinases 1 and 2 exhibit broad-spectrum proteolytic capacities comparable to many matrix metalloproteinases. Eur J Biochem. 250: 751–757.

Dansie LE, and Ethell IM. 2011. Casting a net on dendritic spines: The extracellular matrix and its receptors. Dev Neurobiol. 71: 956–981.

Darnell JC, Van Driesche SJ, Zhang C, Hung KYS, Mele A, Fraser CE, Stone EF, Chen C, Fak JJ, Chi SW, Licatalosi DD, Richter JD, Darnell RB. 2011. FMRP stalls ribosomal translocation on mRNAs linked to synaptic function and autism. Cell. 146: 247-261.

Dityatev A, Brückner G, Dityateva G, Grosche J, Kleene R, Schachner M. 2007. Activity-dependent formation and functions of chondroitin sulfate-rich extracellular matrix of perineuronal nets. Dev Neurobiol. 67: 570-588.

Douglas RJ, Martin, KAC. 2004. Neuronal circuits of the neocortex. Annu Rev Neurosci. 27: 419–451.

Dziembowska M, Pretto DI, Janusz A, Kaczmarek L, Leigh MJ, Gabriel N, Durbin-Johnson B, Hagerman RJ, Tasson F. 2013. High MMP9 activity levels in fragile X syndrome are lowered by minocycline. Am J Med Genet Part A. 161: 1897-1903.

Ehret G. 1976. Development of absolute auditory thresholds in the house mouse (Mus musculus). Ear Hear. 1: 179-184.

Ethell IM, Ethell DW. 2007. Matrix metalloproteinases in brain development and remodeling: synaptic functions and targets. J Neurosci Res. 85: 2813-2823.

Ethridge LE, White SP, Mosconi MW, Wang J, Byerly MJ, Sweeney JA. 2016. Reduced habituation of auditory evoked potentials indicate cortical hyper-excitability in Fragile X Syndrome. Transl Psychiatry. 6: e787.

Gibson JR, Bartley AF, Hays SA, Huber KM. 2008. Imbalance of neocortical excitation and inhibition and altered UP states reflect network hyperexcitability in the mouse model of fragile X syndrome. J Neurophysiol. 100: 2615-2626.

Gkogkas CG, Khoutorsky A, Cao R, Jafarnejad SM, Prager-Khoutorsky M, Giannakas N, Kaminari A, Fragkouli A, Nader K, Price T, Konicek B, Graff J, Tzinia A, Lacaille JC, Sonenberg N. 2014. Pharmacogenetic inhibition of eIF4E-dependent Mmp9 mRNA translation reverses fragile X syndrome-like phenotypes. Cell Rep. 9: 1742-1755.

Gogolla N, Leblanc JJ, Quast KB, Südhof TC, Fagiolini M, Hensch TK. 2009. Common circuit defect of excitatory-inhibitory balance in mouse models of autism. J Neurodev Disord. 1: 172-181.

Gonçalves JT, Anstey JE, Golshani P, Portera-Cailliau C. 2013. Circuit level defects in the developing neocortex of Fragile X mice. Nat Neurosci. 16: 903-909.

Hagerman RJ, Berry-Kravis E, Kaufmann WE, Ono MY, Tartaglia N, Lachiewicz A, Kronk R, Delahunty C, Hessl D, Visootskak J, Picker J, Gane L, Tranfaglia M. 2009. Advances in the treatment of fragile X syndrome. Pediatrics. 123: 378-390.

Hensch TK. 2005. Critical period plasticity in local cortical circuits. Nat Rev Neurosci. 6: 877-888.

Jeevakumar V, Kroener S. 2016. Ketamine administration during the second postnatal week alters synaptic properties of fast-spiking interneurons in the medial prefrontal cortex of adult mice. Cereb Cortex. 26: 1117-1129.

Kim H, Gibboni R, Kirkhart C, Bao S. 2013. Impaired critical period plasticity in primary auditory cortex of fragile X model mice. J Neurosci. 33: 15686-15692.

Kraus HJ, Aulbach-Kraus K. 1981. Morphological changes in the cochlea of the mouse after the onset of hearing. Hear Res. 4: 89-102.

La Fata G, Gärtner A, Domínguez-Iturza N, Dresselaers T, Dawitz J, Poorthuis RB, Averna M, Himmelreich U, Meredith RM, Achsel T, Dotti CG. 2014. FMRP regulates multipolar to bipolar transition affecting neuronal migration and cortical circuitry. Nature Neurosci. 17:1693-700.

Largo RH, Schinzel A. 1985. Developmental and behavioural disturbances in 13 boys with fragile X syndrome. Eur J Pediatr. 143: 269-275.

Lensjø KK, Lepperød ME, Dick G, Hafting T, Fyhn M. 2017. Removal of perineuronal nets unlocks juvenile plasticity through network mechanisms of decreased inhibition and increased gamma activity. J Neurosci. 37: 1269-1283.

Li LY, Ji XY, Liang F, Li YT, Xiao Z, Tao HW, Zhang LI. 2014. A feedforward inhibitory circuit mediates lateral refinement of sensory representation in upper layer 2/3 of mouse primary auditory cortex. J Neurosci. 34: 13670–13683.

Liu H, Gao P-F, Xu H-W, Liu M-M, Yu T, Yao J-P, Yin Z-Q. 2013. Perineuronal nets increase inhibitory GABAergic currents during the critical period in rats. Intl J Ophthalmol. 6: 120.

Lovelace JW, Wen TH, Reinhard S, Hsu MS, Sidhu H, Ethell IM, Binder DK, Razak KA. 2016. Matrix metalloproteinase-9 deletion rescues auditory evoked potential habituation deficit in a mouse model of Fragile X Syndrome. Neurobiol Dis. 89: 126-135.

Martin Del Campo HN, Measor KR, Razak KA. 2012. Parvalbumin immunoreactivity in the auditory cortex of a mouse model of presbycusis. Hear Res. 294: 31-39.

McNaughton CH, Moon J, Strawderman MS, Maclean KN, Evans J, Strupp BJ. 2008. Evidence for social anxiety and impaired social cognition in a mouse model of fragile X syndrome. Behav Neurosci. 122: 293.

McRae PA, Rocco MM, Kelly G, Brumberg JC, Matthews RT. 2007. Sensory deprivation alters aggrecan and perineuronal net expression in the mouse barrel cortex. J Neurosci. 27: 5405–5413.

Miller LJ, McIntosh DN, McGrath J, Shyu V, Lampe M, Taylor AK, Tassone F, Nietzel K, Stackhouse T, Hagerman RJ. 1999. Electrodermal responses to sensory stimuli in individuals with fragile X syndrome. Am J Med Genet. 83: 268-279.

Morawski M, Brückner MK, Riederer P, Brückner G, Arendt T. 2004. Perineuronal nets potentially protect against oxidative stress. Exp Neurol. 188: 309-315.

Morawski M, Reinert T, Meyer-Klaucke W, Wagner FE, Tröger W, Reinert A, Jäger C, Brücker G, Arendt T. 2015. Ion exchanger in the brain: Quantitative analysis of perineuronally fixed anionic binding sites suggests diffusion barriers with ion sorting properties. Sci Rep. 5.

Musumeci SA, Hagerman RJ, Ferri R, Bosco P, Bernardina BD, Tassinari CA, de Sarro GB, Elia M. 1999. Epilepsy and EEG findings in males with fragile X syndrome. Epilepsia. 40: 1092-1099.

Nagy V, Bozdagi O, Matynia A, Balcerzyk M, Okulski P, Dzwonek J, Costa R., Silva A, Kaczmarek L, Huntley GW. 2006. Matrix metalloproteinase-9 is required for hippocampal late-phase long-term potentiation and memory. J Neurosci. 26: 1923–1934.

Natan RG, Briguglio JJ, Mwilambwe-Tshilobo L, Jones SI, Aizenberg M, Goldberg EM, Geffen MN. 2015. Complementary control of sensory adaptation by two types of cortical interneurons. eLife. 4: e09868.

Oswald AMM, Reyes AD. 2011. Development of inhibitory timescales in auditory cortex. Cereb Cortex. 21: 1351–1361.

Paluszkiewicz SM, Olmos-Serrano JL, Corbin JG, Huntsman MM. 2011. Impaired inhibitory control of cortical synchronization in fragile X syndrome. J Neurophysiol. 106: 2264-2272.

Paxinos G, Franklin KBJ. 2004. The mouse brain in stereotaxic coordinates. San Diego (CA): Gulf Professional Publishing.

Pietropaolo S, Guilleminot A, Martin B, D'Amato FR, Crusio WE. 2011. Genetic-background modulation of core and variable autistic-like symptoms in Fmr1 knock-out mice. PLoS One. 6: e17073.

Pizzorusso T, Medini P, Berardi N, Chierzi S, Fawcett JW, Maffei, L. 2002. Reactivation of ocular dominance plasticity in the adult visual cortex. Science. 298: 1248-1251.

Reinhard SM., Razak KA, Ethell IM. 2015. A delicate balance: role of MMP-9 in brain development and pathophysiology of neurodevelopmental disorders. Front Cell Neurosci. 9: 1-16.

Rivera S, Khrestchatisky M, Kaczmarek L, Rosenberg GA, Jaworski DM. 2010. Metzincin proteases and their inhibitors: Foes or friends in nervous system physiology? J Neurosci. 30: 15337–15357.

Roberts JE, Hatton DD, Bailey DB. 2001. Development and behavior of male toddlers with fragile X syndrome. J Early Intervention. 24: 207-223.

Rotschafer S, Razak KA. 2013. Altered auditory processing in a mouse model of fragile X syndrome. Brain Res. 1506: 12–24.

Rubenstein JL, Merzenich MM. 2003. Model of autism: increased ratio of excitation/inhibition in key neural systems. Genes, Brain and Behavior. 2255-67.

Sabaratnam M, Vroegop PG, Gangadharan SK. 2001. Epilepsy and EEG findings in 18 males with fragile X syndrome. Seizure. 10: 60-63.

Saffary R, Xie Z. 2011. FMRP Regulates the Transition from Radial Glial Cells to Intermediate Progenitor Cells during Neocortical Development. J Neurosci. 31: 1427–1439.

Schiff ML, Reyes AD. 2012. Characterization of thalamocortical responses of regular-spiking and fast-spiking neurons of the mouse auditory cortex *in vitro* and *in silico*. J Neurophysiol. 107: 1476–1488.

Selby L, Zhang C, Sun Q-Q. 2007. Major defects in neocortical GABAergic inhibitory circuits in mice lacking the fragile X mental retardation protein. Neurosci Lett. 412: 227–232.

Sidhu H, Dansie LE, Hickmott PW, Ethell DW, Ethell IM. 2014. Genetic removal of matrix metalloproteinase 9 rescues the symptoms of fragile X syndrome in a mouse model. J Neurosci. 34: 9867-9879.

Sinclair D, Oranje B, Razak KA, Siegel, SJ and Schmid S. Sensory processing in autism spectrum disorders and Fragile X syndrome-from the clinic to animal models. 2017. Neurosci & Biobehav Rev. 76: 235-253.

Sohal VS, Zhang F, Yizhar O, Deisseroth K. 2009. Parvalbumin neurons and gamma rhythms enhance cortical circuit performance. Nature. 459: 698–702.

Sugiyama S, Di Nardo AA, Aizawa S, Matsuo I, Volovitch M, Prochiantz A, Hensch TK. 2008. Experience-dependent transfer of Otx2 homeoprotein into the visual cortex activates postnatal plasticity. Cell. 134: 508-520.

Sultan KT, Brown KN, Shi SH. 2013. Production and organization of neocortical interneurons. Front Cell Neurosci. 7: 221.

Tervonen TA, Louhivuroi V, Sun X, Hokkanen ME, Kratochwil CF, Zebryk P, Castrén E, Castrén ML. 2009. Aberrant differentiation of glutamatergic cells in neocortex of mouse model for fragile X syndrome. Neurobiol Dis. 33: 250–259.

Van der Molen, MJW, Van der Molen MW, Ridderinkhof KR, Hamel BCJ, Curfs MLG, Ramakers GJA. 2012. Auditory and visual cortical activity during selective attention in fragile X syndrome: a cascade of processing deficiencies. Clin Neurophysiol. 123: 720-729.

Wang J, Ethridge LE, Mosconi MW, White SP, Binder DK, Pedapati EV, Erickson CA, Byerly MJ, Sweeney JA. 2017. A resting EEG study of neocortical hyperexcitability and altered functional connectivity in fragile X syndrome. J Neurodev Disord. 9: 11.

Winer JA, Miller LM, Lee CC, Schreiner CE. 2005. Auditory thalamocortical transformation: structure and function. Trends Neurosci. 28: 255–263.

Wisniewski KE, Segan SM, Miezejeski CM, Sersen EA, Rudelli, RD. 1991. The Fra (X) syndrome: neurological, electrophysiological, and neuropathological abnormalities. Am J Med Genet. 38: 476-480.

Wlodarczyk J, Mukhina I, Kaczmarek L, Dityatev A. 2011. Extracellular matrix molecules, their receptors, and secreted proteases in synaptic plasticity. Dev Neurobiol. 71: 1040–1053.

Yu S, Pritchard M, Kremer E, Lynch M, Nancarrow J, Baker E, Holman K, Mulley S, Warren T, Schlessinger D, Sutherland GR, Richards RI. 1991. Fragile X Genotype Characterized by an Unstable Region of DNA. Science. 252: 1179-1181.

Zhang Y, Bonnan A, Bony G, Ferezou I, Pietropaolo S, Ginger M, Sans N, Rossier J, Oostra B, LeMasson G, Frick A. 2014. Dendritic channelopathies contribute to neocortical and sensory hyperexcitability in Fmr1-/y mice. Nat Neurosci. 17: 1701-1709.

TABLES

Table 1. PV cell development and PNN formation in the auditory cortex of WT and *Fmr1* KO mice.

	WT		KO	
AGE	**PV+ Cell Density**	**PNN+ Cell Density**	**PV+ Cell Density**	**PNN+ Cell Density**
P14	76.71 ± 4.39	43.55 ± 9.14	53.07 ± 5.07	24.05 ± 7.91
P21	103.42 ± 11.12	59.92 ± 7.21	89.22 ± 5.31	51.71 ± 5.66
P30	92.20 ± 5.86	66.80 ± 6.46	83.00 ± 6.04	83.24 ± 5.18

PV+ and PNN+ cell density in layers 1-4 of WT and KO auditory cortex (average ± SEM). Two-way ANOVA. PV cell density: genotype effect p=0.0317*; age effect p=0.0028**. PNN cell density: genotype effect p=n.s.; age effect p<0.0001**** (Bonferroni post-hoc test: *Fmr1* KO P14 vs. P30, p<0.001; *Fmr1* KO P21 vs. P30, p<0.05). WT N: P14 3 animals/20 slices; P21 7/43; P30 8/59; P60 5/43. KO N: P14 3/22; P21 6/45; P30 7/66.

FIGURES

Figure 1. Layer-specific differences in PV cell density and PNN formation in developing WT and *Fmr1* KO auditory cortex.

(A-F) Confocal images show PV immunoreactivity and WFA-positive PNN labeling in WT and *Fmr1* KO auditory cortex at P14, P21, and P30. Scale bar, 100 µm.

(G-I) High magnification confocal images show examples of cells with PV immunoreactivity and WFA-positive PNN labeling in WT and *Fmr1* KO auditory cortex at P14, P21, and P30. Scale bar, 50 µm.

(J-M) Quantitative analysis of the density of PV cells (J), PNN-containing cells (K), PNN-containing PV cells (L) and percent of PNN-containing PV cells (M) in L2/3 and 4 of WT and KO auditory cortex. (J) In P14 *Fmr1* KO auditory cortex, there was reduced PV cell density in L2/3 (P14 *Fmr1* KO vs. WT, $p<0.0001$) and L4 (P14 *Fmr1* KO vs. WT $p<0.05$). (K) In L4 of auditory cortex, PNN-positive cell density was reduced in P14 *Fmr1* KO mice (*Fmr1* KO vs. WT, $p<0.0001$). (L) The density of PV interneurons enwrapped with PNNs was reduced at P21 in L2/3 (*Fmr1* KO vs. WT; $p<0.01$) and L4 (*Fmr1* KO vs. WT; $p<0.0001$) of *Fmr1* KO auditory cortex as compared to WT. (M) The percent of PV cells containing PNNs was also reduced in L4 of *Fmr1* KO auditory cortex as compared to WT at P21 (*Fmr1* KO vs. WT; $p<0.01$). Statistical analysis was performed using two-way ANOVA with Bonferroni's multiple comparisons post-test (WT N: P14 3 animals/20 slices; P21 7/43; P30 8/59. *Fmr1* KO N: P14 3/22; P21 6/45; P30 7/66; * $p<0.05$; ** $p<0.01$; *** $p<0.001$; **** $p<0.0001$).

Figure 2. PNN formation was selectively impaired around GABAergic interneurons in L4 *Fmr1* KO auditory cortex at P21.

(A) Confocal low magnification image shows GAD65/67 (red) and PV immunoreactivity (blue), and WFA-positive PNN labeling (green) in WT auditory cortex. Scale bar, 100 µm.

(B) Quantitative analysis of the density of PNN-positive GABAergic (GAD65/67 positive) and excitatory (GAD65/67 negative) neurons in L4 of WT and *Fmr1* KO auditory cortex at P21 and P30. (Top) *Fmr1* KO mice showed reduced density of GABAergic interneurons enwrapped with PNNs in L4 auditory cortex as compared to WT at P21 (**$p<0.01$). (Bottom) There was a developmental increase in GAD-negative cells enwrapped with PNNs (P21 vs. P30; **$p<0.01$), but there were no genotype-specific differences. Statistical analysis was performed using two-

way ANOVA with Bonferroni multiple comparisons post-test (WT N: P21 3 animals/12 slices; P30 3/26. *Fmr1* KO N: P21 3/20; P30 3/12).

(C, D) Confocal high magnification images of net structures exemplifying PNNs that surround PV, GAD+ and GAD- cells in WT and *Fmr1* KO auditory cortex at P21 (C) and P30 (D). Scale Bar, 100 µm. * indicates a GAD+/PV+ cell (purple) without PNN, arrows indicate GAD+/PV+ cells with PNN, arrowheads indicate GAD-/PV- cells with PNNs.

Figure 3. Detection of MMP-9 and MMP-2 levels in the developing auditory cortex.

(A, D) Detection of MMP-9 and MMP-2 levels using gelatin zymography.

(B, C) Graph shows MMP-9 (B) and MMP-2 (C) levels in WT and *Fmr1* KO auditory cortex at P3, P7, P12 and P18 (values were quantified by densitometry and normalized to the P7 WT value). (B) Levels of MMP-9 peak at P7 and decrease with age during auditory cortex development in WT mice; however compared to WT levels MMP-9 levels are elevated in *Fmr1* KO mice at all ages ($p < 0.01$). (C) MMP-2 levels also showed a developmental downregulation from P3 to P18 (Fig. 4C; $p<0.05$) but levels were similar between WT and *Fmr1* KO mice at all ages (Fig. 4C; p = n.s.). Statistical analysis was performed using two-way ANOVA with Bonferroni's multiple comparisons post-test (WT N: 6, 8, 4 and 4 mice. *Fmr1* KO N: 6, 8, 4 and 4 mice).

(E, F) Graph shows MMP-9 (E) and MMP-2 (F) levels in WT, *Fmr1* KO and MMP-9+/-*Fmr1* KO auditory cortex at P12 (values for MMP-9+/-*Fmr1* KO and *Fmr1* KO samples were normalized against values for WT sample with similar protein concentration run on the same gel). Levels of MMP-9 were significantly higher in *Fmr1* KO (*$p<0.05$) but not MMP-9+/-*Fmr1* KO auditory cortex as compared to WT, whereas MMP-9 levels were significantly lower in MMP-

9+/-*Fmr1* KO auditory cortex as compared to *Fmr1* KO (*p<0.01). Statistical analysis was performed using one-way ANOVA with Bonferroni multiple comparisons post-test (WT N: 9 mice, *Fmr1* KO N: 9 mice and MMP-9+/-*Fmr1* KO N: 6 mice).

Figure 4. Genetic MMP-9 reduction promotes PNN formation around PV interneurons in L4 *Fmr1* KO auditory cortex at P21.

(A-C) Confocal images of PV (red) and WFA-positive PNN-containing (green) cells in L4 auditory cortex of WT, *Fmr1* KO, and *Mmp9*+/-*Fmr1* KO mice at P21. Mmp9+/- *Fmr1* KO brain samples were collected and analyzed together with experimentally matched WT and KO groups. Scale Bar, 100 μm. White * indicates a PV cell without PNN, white arrows indicate PV cells with PNN.

(D-G) Quantitative analysis of the density of PV cells (D), PNN-containing cells (E), PNN/PV expressing cells (F) and percent of PNN-containing PV cells (G) in L4 auditory cortex of WT, *Fmr1* KO, and *Mmp9*+/-*Fmr1* KO at P21. (D) PV cell density was reduced in *Fmr1* KO auditory cortex as compared to WT (*Fmr1* KO vs. WT p<0.01). (E) PNN cell density was reduced in Fmr1 KO mice (*p<0.05) but was significantly higher in *Mmp9+/-Fmr1* KO mice compared to KO (****p<0.001). (F) PNN/PV cell density was reduced in Fmr1 KO compared to WT cortex (****p<0.0001), but was significantly higher in *Mmp9+/-Fmr1* KO compared to KO (**p<0.01). (G) *Fmr1* KO mice showed reduced percentage of PV cells with PNNs but not after MMP-9 reduction in *Mmp9+/-Fmr1 KO* mice (WT vs. Fmr1 KO, ****p<0.0001; *Mmp9+/-Fmr1* KO vs. *Fmr1* KO, ***p<0.01). Statistical analysis was performed using one-way ANOVA with Bonferroni's multiple comparisons post-test, and Kruskal-Wallis one-way analysis of ranks for data which was not normally distributed (WT N: P21 3 animals/22 slices; *Fmr1* KO N: P21 3/17; *Mmp9*+/-*Fmr1* KO N: P21 3/24).

Figure 5. Response magnitudes and spontaneous activity are enhanced in P21 *Fmr1* KO auditory cortex.

(A, D) PSTHs showing example responses within 200ms from the onset of a 50ms pure tone stimulus (black bar) played at the CF, 15 dB above threshold in a WT (top) and a *Fmr1* KO neuron (bottom) at P14 (A) or P21 (D).

(B, C) Analysis shows increased spikes/stimulus in the ongoing response (C) but not the first 50ms onset response (B) in *Fmr1* KO auditory cortex as compared to WT at P21 but not P14 (P21 WT vs. *Fmr1* KO, **p<0.01). Additionally, response magnitude increases in *Fmr1* KO auditory cortex with age but not in WT (*Fmr1* KO P14 -> P21, p<0.001).

(E) Genotype and age differences at P21 were also evident when the response magnitude was measured across the entire 200 ms recording window (P21 WT vs. *Fmr1* KO, **p<0.01; *Fmr1* KO P14 -> P21, **p<0.01). (F) Spontaneous activity was also significantly higher in *Fmr1* KO auditory cortex at P21 but not P14. Statistical analysis was performed using two-way ANOVA with Bonferroni's multiple comparisons post-test. (For response magnitude, P14 WT N=73 neurons, KO N=85 neurons; P21 WT N=89 neurons, KO N=92 neurons. For spontaneous activity, P14 WT N=67, KO N=83; P21 WT N=88 neurons, KO N=91 neurons.)

Figure 6. Genetic reduction of MMP-9 restores response magnitudes in *Fmr1* KO mice to WT levels.

(A) PSTHs showing example responses within 200ms from the onset of a 50 ms pure tone stimulus (black bar) played at the CF, 15 dB above threshold in a WT (top), *Fmr1* KO (middle), and *Mmp9*+/- *Fmr1* KO neuron (bottom).

(B, C) Graphs show the first 50ms onset response (B) and the 51-200ms ongoing response (C). There is increased spikes/stimulus in the ongoing response (C) in *Fmr1* KO mice, which is restored to WT levels with genetic reduction of MMP-9 (**p<0.01 WT vs. *Fmr1* KO, ***p<0.001 *Fmr1* KO vs. *Mmp9+/- Fmr1* KO).

(D) Across the entire 200ms recording window, the mean spikes per stimulus presentation, averaged over 20 stimulus presentations, is increased in *Fmr1* KO neurons and restored to WT levels with genetic reduction of MMP-9 (WT vs. *Fmr1* KO, **p<0.01; *Fmr1* KO vs. *Mmp9+/- Fmr1* KO, ***p<0.001).

(E) Spontaneous activity is increased in *Fmr1* KO mice and restored to WT levels with genetic reduction of MMP-9. Statistical analysis was performed using Kruskal-Wallis one-way analysis of ranks with Dunnett's C for post-hoc analysis (for response magnitude, WT N: 12 animals/89 neurons; *Fmr1* KO N: 13 animals/92 neurons; *Mmp9+/- Fmr1* KO N: 12 animals/107 neurons. For spontaneous activity, WT N: 12 animals/88 neurons; *Fmr1* KO N: 13 animals/91 neurons; *Mmp9+/- Fmr1* KO N: 12 animals/106 neurons).

Figure 7. Working model of the effects of MMP-9 reduction on PNN formation in auditory cortex of the *Fmr1* KO mice.

(Left) In WT animals, there is normal production of FMRP, which translationally suppresses MMP-9 production, resulting in normal development and maturation of PV interneurons (white) and PNNs (black) and normal neural excitability. (Middle) *Fmr1* KO results in loss of FMRP and upregulated production of MMP-9. High MMP-9 levels lead to the enhanced cleavage and loss of PNNs around PV cells and alters E/I balance. (Right) PNN formation is enhanced around PV cells following genetic reduction of MMP-9 in the *Fmr1* KO mice, resulting in normal

density of PNN-containing PV cells and reduced excitability in *Mmp9*+/-*Fmr1* KO auditory cortex as compared to *Fmr1* KO mice.

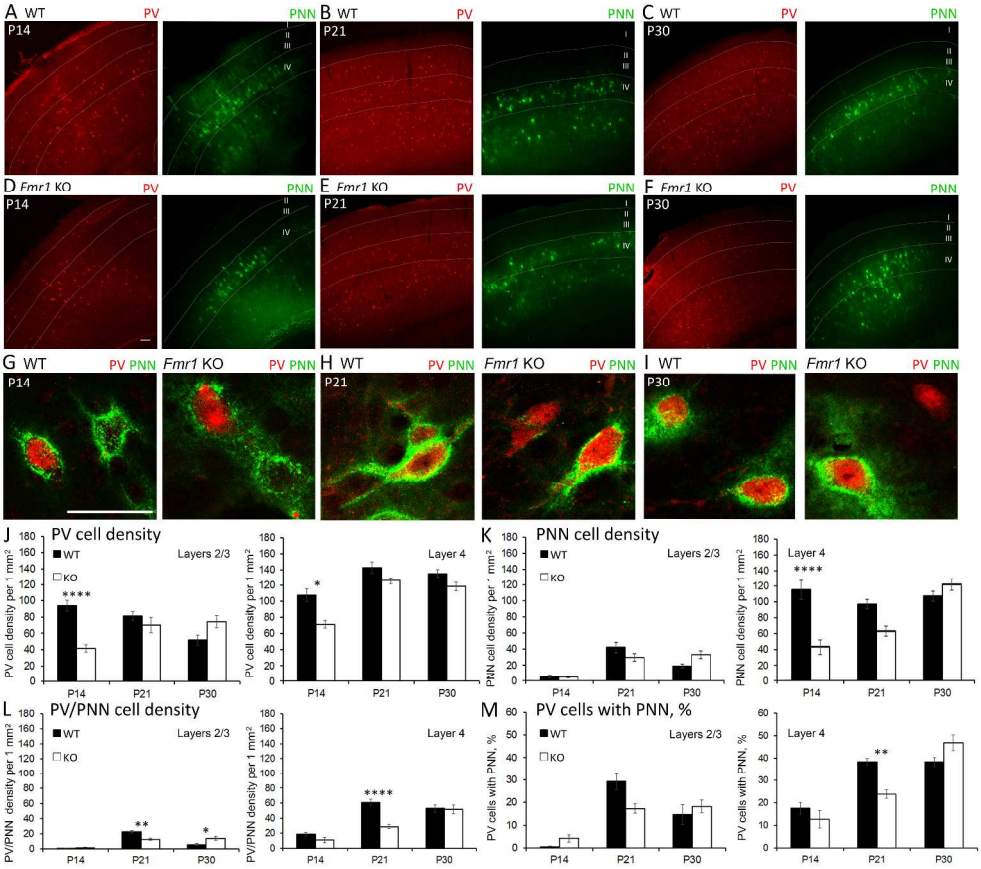

Figure 1. Layer-specific differences in PV cell density and PNN formation in developing WT and Fmr1 KO auditory cortex.

566x493mm (300 x 300 DPI)

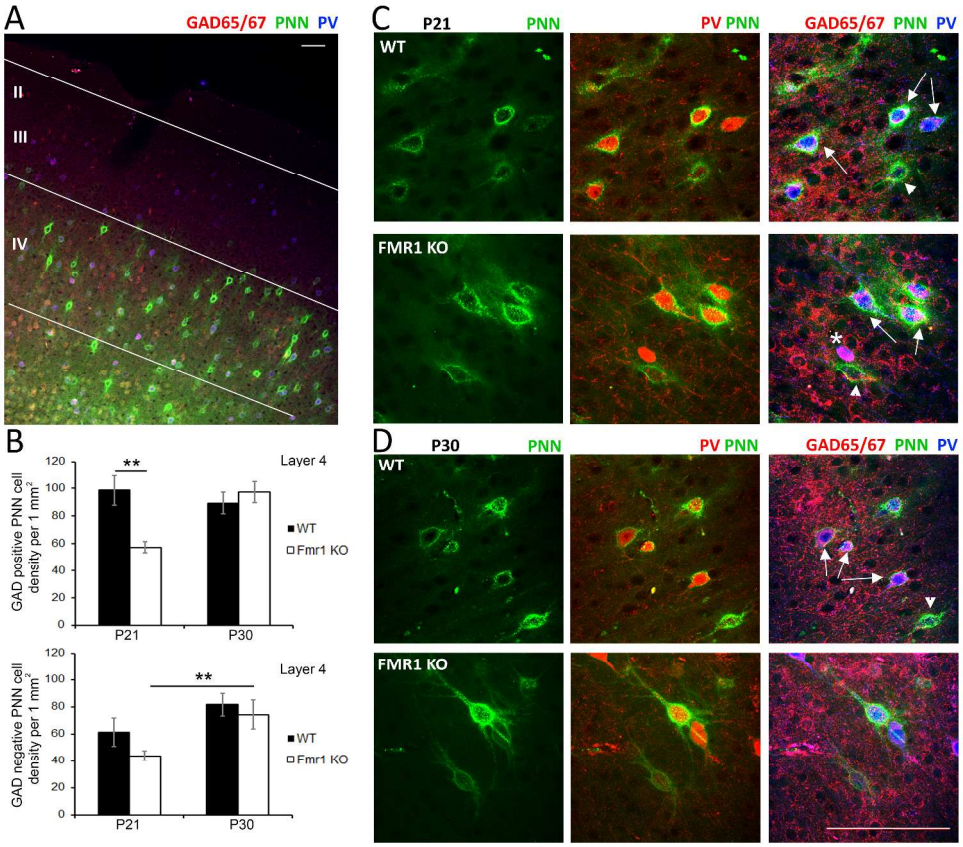

Figure 2. PNN formation was selectively impaired around GABAergic interneurons in L4 Fmr1 KO auditory cortex at P21.

457x402mm (300 x 300 DPI)

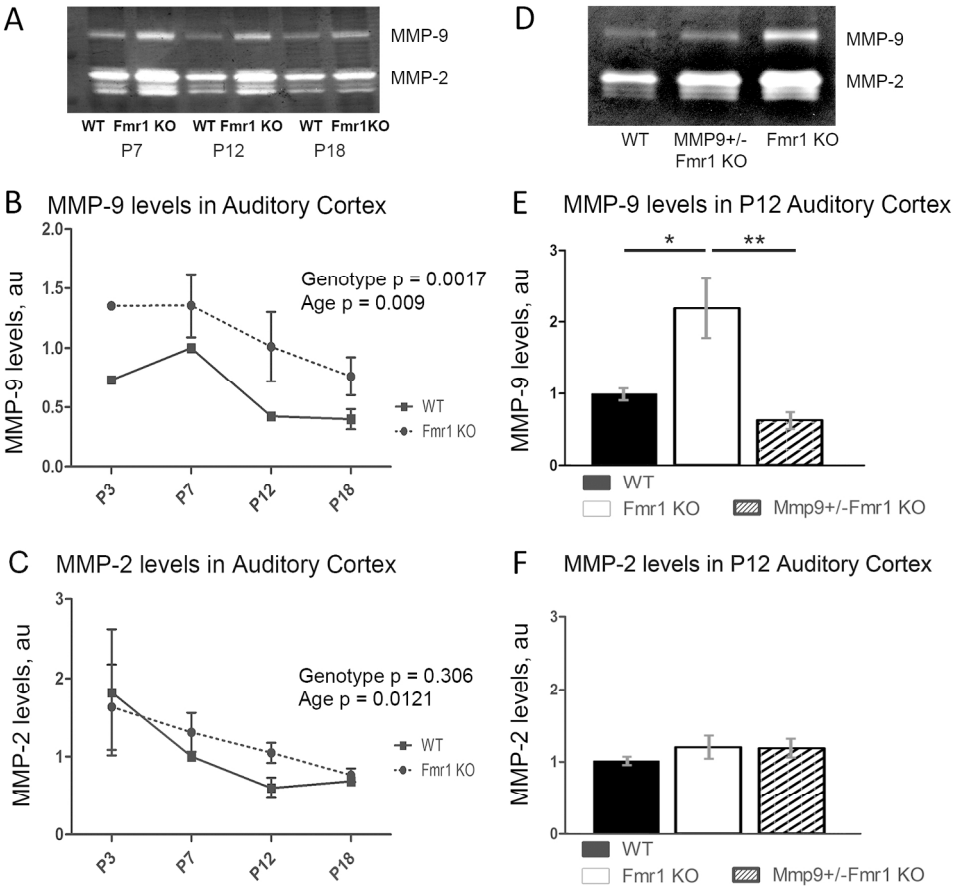

Figure 3. Detection of MMP-9 and MMP-2 levels in the developing auditory cortex.

170x157mm (300 x 300 DPI)

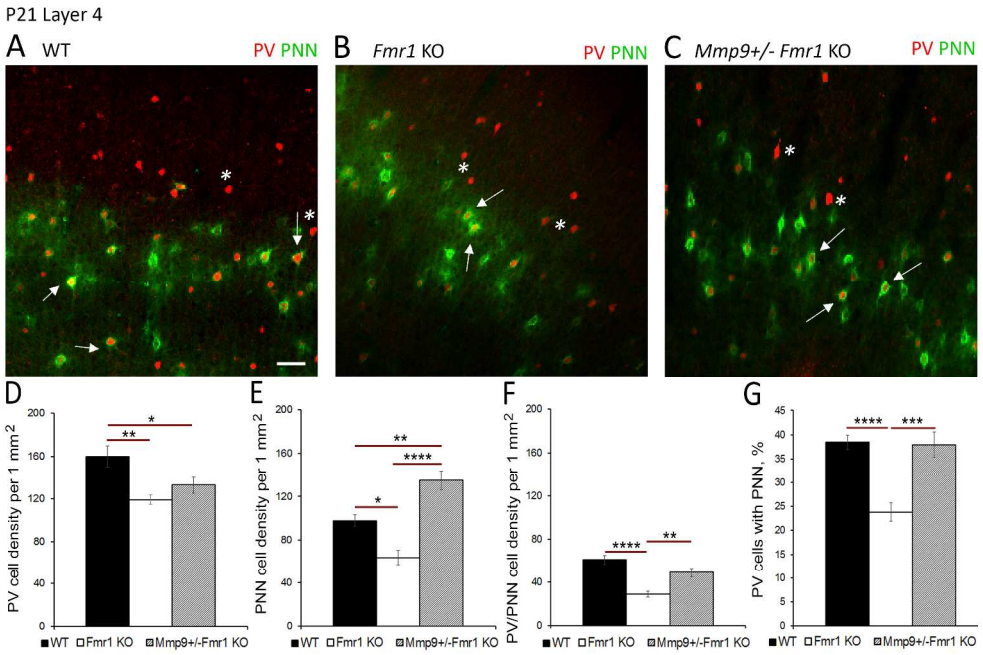

Figure 4. Genetic MMP-9 reduction promotes PNN formation around PV interneurons in L4 Fmr1 KO auditory cortex at P21.

304x204mm (300 x 300 DPI)

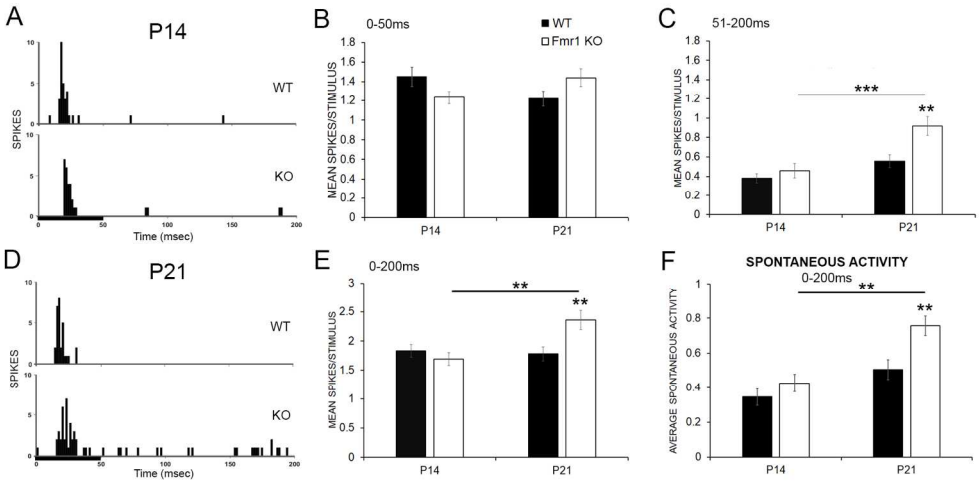

Figure 5. Response magnitudes and spontaneous activity are enhanced in P21 Fmr1 KO auditory cortex.

162x78mm (300 x 300 DPI)

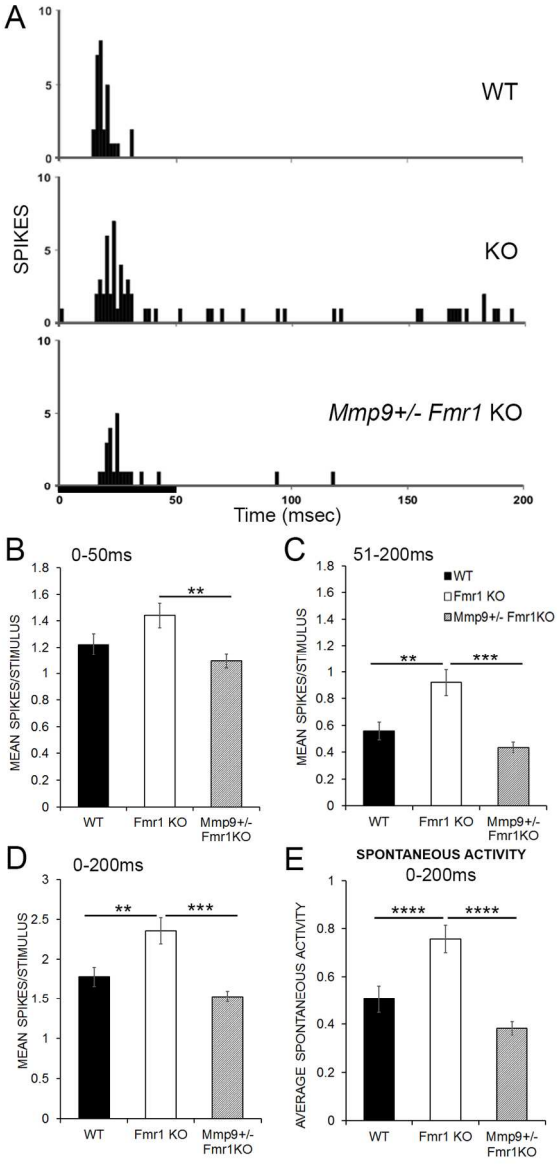

Figure 6. Genetic reduction of MMP-9 restores response magnitudes in Fmr1 KO mice to WT levels.

89x186mm (300 x 300 DPI)

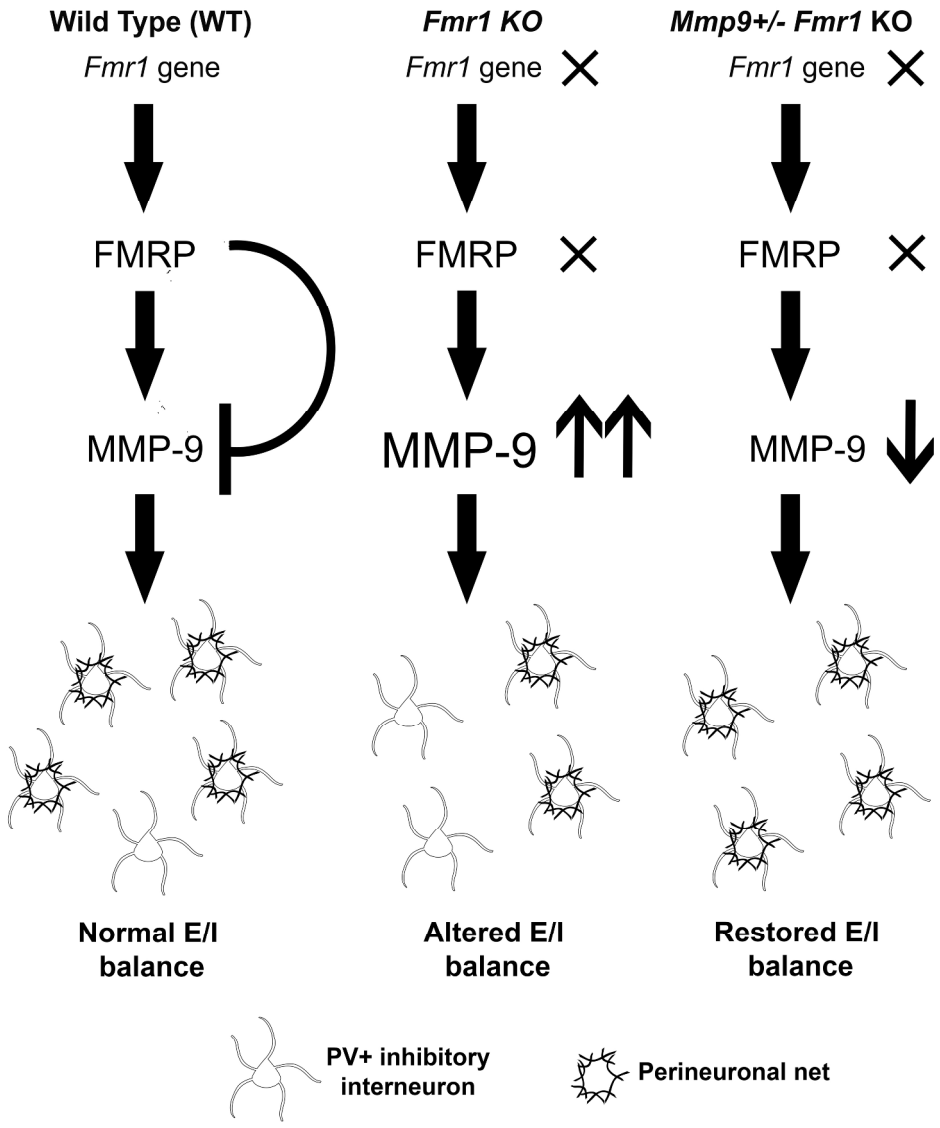

Figure 7. Working model of the effects of MMP-9 reduction on PNN formation in auditory cortex of the Fmr1 KO mice.

262x302mm (300 x 300 DPI)

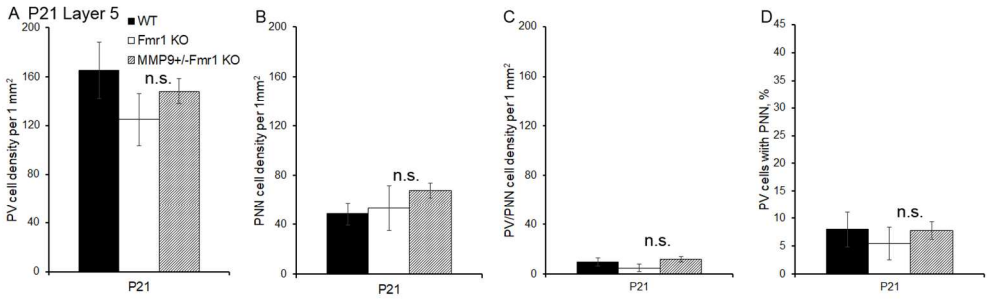

Supplementary Figure 1. PV cell density and PNN formation are not altered in layer 5 of P21 Fmr1 KO auditory cortex.
(A-D) Quantitative analysis of the density of PV cells (A), PNN-containing cells (B), PNN-containing PV cells (C) and percent of PNN-containing PV cells (D) in L5 of WT, KO, and Mmp9+/-Fmr1 KO auditory cortex. Statistical analysis was performed using Kruskal-Wallis one-way analysis of ranks (WT N: 3/22; Fmr1 KO N: 3/17; Mmp9+/-Fmr1 KO N: 3/24).

125x39mm (300 x 300 DPI)